Continuous and Discrete Phase-shifts for RIS-aided Systems in Wideband Communication Channels

Pedro H. C. Souza, Masoud Khazaee and Luciano Mendes

***Abstract*— This work investigates the performance of the reconfigurable intelligent surface (RIS) for wideband communication systems, also considering line of sight (LOS) channels. We evaluate the achievable rate of methods such as the alternating optimization (AO) and strongest tap maximization (STM), which are used to configure the RIS. Additionally, the impact of continuous and discrete phase-shifts is also analyzed in the context of novel proposed metrics, denoted as the relative and efficiency rate. It is demonstrated that discrete or quantized phase-shifts can achieve a rate close to that of continuous phase-shifts, if enough quantization bits are used.**

***Keywords*— RIS, wideband, alternating optimization, strongest tap maximization, discrete phase-shifts, quantization.**

I. Introduction

The modern society is now experiencing a rapid transition to a complete digital and heterogeneous ecosystem of communication devices and, at the same time, an exponential increase in wireless communication usage. As a response to these demands, the recent advent of the sixth generation of mobile network (6G) systems bring novel key enabling technologies such as terahertz communications, cell-free massive multiple-input multiple-output (MIMO) and many others [1]. More importantly, 6G systems will enable the so-called intelligent communication environments, with efforts toward the advancement of wireless transceiver hardware and software, network optimization strategies, and also the improvement of the wireless communication environment, by actively controlling how the electromagnetic waves interact with the propagation medium [1], [2].

The signal propagation control can involve several aspects as, for example, the wave reflection, absorption, polarization and so forth [1]. However, in this work, we focus on controlling it by means of the reconfigurable intelligent surface (RIS), which is concerned solely with the reflection aspect. The RIS is typically a planar surface constituted by metamaterials tiles and can be modeled mathematically by a collection of elements or reflectors that apply phase-shifts on the impinging signal and reradiate it without amplification or regeneration [1], [2]. This modeling is also denoted as a reflectarray. One of the main problem lies, however, in finding the optimum pattern of phase-shifts or RIS configuration for a given performance metric, such as maximizing the signal power at the intended receiver.

Pedro H. C. Souza, Masoud Khazaee and Luciano Mendes, Inatel, Sta. Rita do Sapucaí-MG, e-mails: pedro.carneiro@dtel.inatel.br, {masoud@ and luciano@}inatel.br. This work was partially funded by Brasil 6G Project (RNP/MCTI no 01245.020548/2021-07), SAMURAI project (FAPESP grant 20/05127-2), and by the project Advanced Academic Education in Telecommunications Networks and Systems (Huawei PPA6001BRA23032110257684).

Therefore, in this work we discuss different methods for doing so, also considering wideband channels and the particular set of challenges brought by them. Additionally, we discuss the practical case where there is a finite number of phase shift configurations available [3], [4]. This represents a scenario where phase-shifts are discrete, instead of the commonly assumed continuous RIS configuration. Although other works [5]–[7] study the impact of discrete or quantized phase-shifts on various aspects of the RIS implementation, yet, in this work, we analyze it considering wideband channels. Furthermore, we also propose novel metrics to evaluate the performance and complexity trade-off of discussed RIS configuration methods.

This work is organized as follows: Section II presents the channel modeling and unveils the relevant details about the RIS configuration, Section III describes all channel model parameters and presents the performance results and Section IV concludes the paper.

II. System Model

A. Channel Model

Consider a micro-cell where both a transmitting access point (AP) and a receiving user equipament (UE) are located. To aid the signal transmission between the AP and UE, we assume the use of a RIS containing N reflectors or elements, which can be represented mathematically by $\boldsymbol{\omega}_\theta = e^{j\boldsymbol{\theta}} \in \mathbb{C}^N$, where $\boldsymbol{\theta} = [\theta_0, \theta_1, \ \ldots, \theta_{N-1}]^{\mathrm{T}}$. Therefore, note in Figure 1 that the

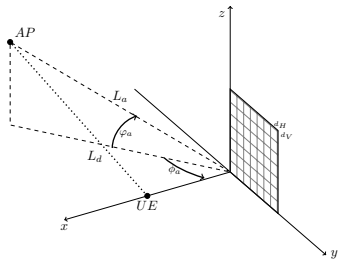

Fig. 1. Spatial diagram of the system model on a $(x,\ y,\ z)$ coordinate system.

propagation environment is composed of a direct channel with L_d paths between the AP and UE, which are all assumed to be in the line of sight (LOS). Additionally, there is the composite channel, composed by the cascade of the channels between the AP and RIS (L_a paths) and RIS to the UE (L_b paths), also assumed to be LOS channels.

Since a three-dimensional space is considered, then the relative azimuth angles of arrival (ϕ_a) and departure (ϕ_b) at/from the RIS, as well as the respective elevation angles φ_a and φ_b, are also taken into account, as illustrated in Figure 1

for the L_a channel. The same is applied for the L_b channel but is omitted in Figure 1 for convenience. These angles affect the so-called spacial signature of the propagation model and interact with the positioning of the planar RIS elements, each one having sides of size d_{H} and d_{V} meters. Consequently, the spacial signature considering the L_a channel can be given by

$$\mathcal{S}\left(\Phi_a\right) = e^{\jmath \boldsymbol{\phi}_a^{l\,\mathrm{T}} \Psi}, \text{ with } \Psi = [\mathbf{0}, \Psi_{\mathrm{H}}, \Psi_{\mathrm{V}}]^{\mathrm{T}}, \tag{1}$$

where $l \in \{1, \ldots, L_a\}$ and furthermore we have

$$\Phi_a^l = \frac{-2\pi}{\lambda} \left[\cos\left(\phi_a^l\right)\cos\left(\varphi_a^l\right), \sin\left(\phi_a^l\right)\cos\left(\varphi_a^l\right), \sin\left(\varphi_a^l\right)\right]^{\mathrm{T}}, \tag{2}$$

in which $\lambda = 3 \times 10^8 f_c^{-1}$, f_c being the central frequency of the signal carrier. Finally, consider the following

$$\Psi_{\mathrm{H}} = d_{\mathrm{H}} \left[\mathrm{mod}(0/N_{\mathrm{row}}), \mathrm{mod}\left(1/N_{\mathrm{row}}\right), \ldots, \mathrm{mod}\left(N-1/N_{\mathrm{row}}\right)\right]^{\mathrm{T}}; \tag{3}$$

$$\Psi_{\mathrm{V}} = d_{\mathrm{V}} \left[\lfloor 0/N_{\mathrm{col}} \rceil, \lfloor 1/N_{\mathrm{col}} \rceil, \ldots, \lfloor N-1/N_{\mathrm{col}} \rceil\right]^{\mathrm{T}}, \tag{4}$$

wherein $\mathrm{mod}(\cdot)$ is the modulo operation and $\lfloor \cdot \rceil$ rounds a number to the nearest integer. Therefore, $\Psi \in \mathbb{C}^{3\times N}$ can be seen as the area spanned by the RIS planar surface across the $y-z$ plane, as illustrated in Figure 1, for which $N = N_{\mathrm{row}} N_{\mathrm{col}}$. The same formulation of (1) is employed for the L_b channel and the RIS orientation could be modified without loss of generality.

In this work, we study the scenario for which there are K subcarriers transmitting the signal, using an orthogonal frequency division multiplex (OFDM) system. This scenario is notoriously challenging for the RIS feasibility, in the sense that there is no unique $\boldsymbol{\omega}_\theta$ for all different subcarriers [2]. To elaborate, first let the m-th sample of the composite channel be written as in:

$$h\left[m\right] = \sum_{n=0}^{N-1} \sum_{l=1}^{L_a} \sum_{\ell=1}^{L_b} \sqrt{\alpha^l \beta^\ell} \mathcal{S}\left(\Phi_a\right) \mathcal{S}\left(\Phi_b\right) \times e^{-\jmath 2\pi f_c \left(\tau_a^l + \tau_b^\ell + \tau_{\theta_n}\right)} s\left(m\right); \tag{5}$$

in which,

$$s\left(m\right) = \mathrm{sinc}\left(m + B\left(\eta - \tau_a^l - \tau_b^\ell + \tau_{\theta_n}\right)\right), \tag{6}$$

and where α^l and β^ℓ are, respectively, the propagation losses for the L_a and L_b channels, $\mathcal{S}\left(\Phi_a\right)$ and $\mathcal{S}\left(\Phi_b\right)$ are given by (1), τ_a^l and τ_b^ℓ are the propagation delays, whereas $\tau_{\theta_n} = \theta_n / 2\pi f_c$ is the phase shift caused by the n-th RIS element. Furthermore, B is the bandwidth occupied by all subcarriers, for which we assume that each subcarrier is ascribed to a fixed bandwith value. Also note that $\eta = \min\left(\tau_d^l\right)$, $\forall l \in L_d$, to assure causality. Bear in mind that the coefficients of the impulse response associated with the composite channels are defined within (5), in particular by the parameters α^l, β^ℓ, τ_a^l, τ_b^ℓ; for all $l \in L_a$ and $\ell \in L_b$. Likewise, the direct channel, $h_d[m]$ $\forall m$, is described similarly to (5) and is omitted here for the sake of brevity.

B. RIS Configuration

The problem then resides in configuring all the RIS elements accordingly, so that the signal power is increased at the UE or the channel capacity is maximized. This is achieved when both the direct and composite channels combine constructively at the UE, with their respective phases aligned. However, for the wideband scenario analysed in this work, keep in mind that the signal is transmitted simultaneously across all K subcarriers, whilst each subcarrier presents different channel properties as, for example, phase-shifts. That way, the RIS is unable to configure a different $\boldsymbol{\omega}_\theta$ for each subcarrier, and a nontrivial trade-off must be achieved between all subcarriers. Consider the following:

$$\mathbf{F}\left[h\left[0\right], h\left[1\right], \ldots, h\left[M-1\right]\right]^{\mathrm{T}} = \mathbf{F}\mathbf{V}^{\mathrm{T}}\boldsymbol{\omega}_\theta; \tag{7}$$

where M is the total number of time samples and $\mathbf{F} \in \mathbb{C}^{K\times M}$ is the the discrete Fourier transform (DFT) matrix, whose elements are represented by $F_{i,j} = e^{-\jmath 2\pi ij/K}$. Moreover, $\mathbf{V} = [\mathbf{v}_0, \mathbf{v}_1, \ \ldots, \mathbf{v}_{N-1}]^{\mathrm{T}} \in \mathbb{C}^{N\times M}$ describes all N composite channels, for which phases are subsequently modified by the configured RIS phase-shifts $\boldsymbol{\omega}_\theta$. Therefore, note in (7) that the same N phase-shifts operate all K subcarriers.

The problem of finding the best configuration for the RIS phase-shifts ultimately can be described in terms of the channel capacity maximization [2]–[4], [8], according to which the achievable rate is formulated as follows

$$R = \frac{B}{\xi} \overbrace{\sum_{i=0}^{K-1} \log_2\left(1 + \frac{p_i \|\mathbf{f}_i^{\mathrm{H}}\mathbf{h}_d + \mathbf{f}_i^{\mathrm{H}}\mathbf{V}^{\mathrm{T}}\boldsymbol{\omega}_\theta\|_2^2}{BN_0}\right)}^{\mathcal{R}} \ \mathrm{bit/s}, \tag{8}$$

wherein $\xi = K + M - 1$, to take into account the cyclic prefix loss[1], $\mathbf{p} \in \mathbb{R}^K$ is the power allocated to the k-th subcarrier, such that $P = \langle \mathbf{p} \rangle$; P being the total transmission power[2], $\mathbf{f}_i$ represents the i-th row of the DFT matrix $\mathbf{F}$, B is the total bandwidth occupied by K subcarriers, and N_0 is the additive white Gaussian noise (AWGN) power.

1) Convex Optimization: In order to perform the RIS configuration, one alternative is to cast the capacity maximization problem as a convex optimization problem [3], [4], [8]. Firstly, let the achievable rate of (8) be rewritten as an objective function of a general optimization problem, such that

$$\begin{aligned} &\underset{\mathbf{p},\boldsymbol{\omega}_\theta}{\text{maximize}} \ \mathcal{R} \\ &\text{subject to } \langle \mathbf{p} \rangle \leq P, \\ &\qquad p_i \geq 0\ , \qquad \forall i \in \{0,1,\ldots,K-1\}, \\ &\qquad \|\omega_{\theta_n}\|_2^2 \leq 1\ , \ \forall n \in \{0,1,\ldots,N-1\}. \end{aligned} \tag{9}$$

However, (9) is a non-convex optimization problem, thus motivating the formulation of the following equivalent convex

[1]The cyclic prefix duration ensures that $M - 1 > B\tau_{\max}$, where $\tau_{\max}$ is the largest propagation delay (see Table I).

[2]$\langle \mathbf{p} \rangle = K^{-1} \sum_k p\left[k\right]$

problem [8]

$$\begin{aligned} \underset{\boldsymbol{\omega}_\theta,\{y_i\},\{a_i\},\{b_i\}}{\text{maximize}} \quad & \sum_{i=0}^{K-1} \log_2\left(1+\frac{p_i y_i}{BN_0}\right) \\ \text{subject to} \quad & \|\omega_{\theta_n}\|_2^2 \leq 1 \ , \qquad \forall n \ , \\ & a_i = \Re\{\mathbf{f}_i^{\mathrm{H}}\mathbf{h}_d + \mathbf{f}_i^{\mathrm{H}}\mathbf{V}^{\mathrm{T}}\boldsymbol{\omega}_\theta\} \ , \ \forall i \ , \\ & b_i = \Im\{\mathbf{f}_i^{\mathrm{H}}\mathbf{h}_d + \mathbf{f}_i^{\mathrm{H}}\mathbf{V}^{\mathrm{T}}\boldsymbol{\omega}_\theta\} \ , \ \forall i \ , \\ & y_i \leq f_i\left(a_i, b_i\right) \ , \qquad \forall i \ . \end{aligned} \tag{10}$$

where,

$$f_i\left(a_i, b_i\right) = \tilde{a}_i^2 + \tilde{b}_i^2 + 2\tilde{a}_i(a_i - \tilde{a}_i) + 2\tilde{b}_i(b_i - \tilde{b}_i) \tag{11}$$

and for which the power allocation, $\mathbf{p}$, and the RIS phase-shifts, $\boldsymbol{\omega}_\theta$, are jointly optimized. More specifically, the joint optimization is performed by way of the alternating optimization (AO) framework [3], [4], where an approximate solution to (9) is reached by iteratively optimizing each variable $\mathbf{p}$ or $\boldsymbol{\omega}_\theta$ at a time, that is, one of these variables is optimized while the other maintains a fixed value. This framework can be described by Algorithm 1.

Algorithm 1 The alternating optimization framework

Require: $\mathbf{h}_d$, $\mathbf{V}$, $\mathbf{F}$, K, N and $\boldsymbol{\omega}_\theta^{\text{initial}}$
Ensure: $\tilde{a}_i = \Re\{\mathbf{f}_i^{\mathrm{H}}\mathbf{h}_d + \mathbf{f}_i^{\mathrm{H}}\mathbf{V}^{\mathrm{T}}\boldsymbol{\omega}_\theta^{\text{initial}}\} \ , \ \forall i$
Ensure: $\tilde{b}_i = \Im\{\mathbf{f}_i^{\mathrm{H}}\mathbf{h}_d + \mathbf{f}_i^{\mathrm{H}}\mathbf{V}^{\mathrm{T}}\boldsymbol{\omega}_\theta^{\text{initial}}\} \ , \ \forall i$
Ensure: $\mathcal{R}^* \leftarrow \infty$
repeat
  $\mathcal{R} \leftarrow \mathcal{R}^*$
  Find the optimum $\mathbf{p}^*$ (e.g. water filling algorithm [9])
  $\boldsymbol{\omega}_\theta^* \leftarrow \infty$
  repeat
    $\boldsymbol{\omega}_\theta \leftarrow \boldsymbol{\omega}_\theta^*$
    Find $\boldsymbol{\omega}_\theta^*$ by solving (10) (e.g. CVXPY [10])
    $\tilde{a}_i = a_i$, $\tilde{b}_i = b_i \ , \ \forall i$
  until $|\boldsymbol{\omega}_\theta^* - \boldsymbol{\omega}_\theta| \sim 0$
  $\mathcal{R}^* \leftarrow \sum_{i=0}^{K-1} \log_2\left(1 + {p_i}^* \|\mathbf{f}_i^{\mathrm{H}}\mathbf{h}_d + \mathbf{f}_i^{\mathrm{H}}\mathbf{V}^{\mathrm{T}}\boldsymbol{\omega}_\theta^*\|_2^2/BN_0\right)$
until $|\mathcal{R}^* - \mathcal{R}| \sim 0$

Note that this algorithm employs the successive convex approximation (SCA) technique [3], [4], [8] to solve (10) and also the well-known water filling algorithm [2], [8], [9] to calculate the optimum power allocation. Moreover, the initial phases used for calculating the first power allocation values can be defined according to a heuristic method [8], given by

$$\boldsymbol{\omega}_{\theta_n}^{\text{initial}} = e^{-\jmath \arg\left\{\left(\mathbf{h}_d^{\mathrm{H}} + \sum_{u\neq n} \mathbf{v}_u^{\mathrm{H}}\boldsymbol{\omega}_{\theta_u}^{\text{initial}}\right)\mathbf{v}_n\right\}} \ , \ \forall n, \tag{12}$$

which is essentially a successive phase alignment operation that computes the phase-shifts sequentially, starting from a set of initial random phases with unit amplitudes.

2) Strongest Tap Maximization: Although the AO framework computes near-optimum RIS configurations according to the channel capacity maximization, yet it is costly in terms of computational complexity [2]. On the other hand, the strongest tap maximization (STM) builds upon the premise that typically most of the received signal power is concentrated in a few time-domain samples [2]. For channels with a strong LOS propagation path, for example, most of the signal power is concentrated in a few taps or time samples. In other words, usually $M \ll K$, and thus to reach a RIS configuration considering M samples may become more straightforward than finding an optimum trade-off for $\boldsymbol{\omega}_\theta$ considering all K subcarriers.

To elaborate, let us define the STM as

$$\boldsymbol{\omega}_\theta^{m^*} = \underset{m\in\{0,1,\ldots,M-1\}}{\arg\max} \|h_d\left[m\right] + \mathbf{V}_m^{\mathrm{T}}\boldsymbol{\omega}_\theta^m\|_2^2, \tag{13}$$

where $\mathbf{V}_m$ is the m-th row of $\mathbf{V}$ and also

$$\boldsymbol{\omega}_{\theta_n}^m = e^{\jmath(\arg\{h_d[m]\} - \arg\{V_{m,n}\})} \ , \ \forall n \in \{0,1,\ldots,N-1\}, \tag{14}$$

which represents the alignment of phase-shifts for all N RIS elements, such that the direct channel, $\mathbf{h}_d$, combines in-phase with the composite channel, $\mathbf{V}$, for the m-th time sample. This means that $\boldsymbol{\omega}_\theta^{m^*}$ is the RIS configuration that results in the largest magnitude of the received time-domain signal and, consequently, that m^* is the time instant from which this configuration is based.

III. Numerical Results

In this section, we discuss the performance of different RIS configuration methods or approaches for the wideband scenario.

A. System Parameters

Firstly, we summarized in Table I the values and definitions ascribed to all fixed parameters of the channel model presented in Subsection II-A. For ease of presentation, Table I is arranged into three main columns, one describing the so-called general parameters and the others being denoted as the channel parameters columns.

It is assumed that the AP as well as the UE have fixed coordinates, as shown by the tuples in Table I, that is, $(x_a,\ y_a,\ z_a)$ and $(x_b,\ y_b,\ z_b)$, respectively. Moreover, note that the path delays τ_a^l and τ_b^ℓ have their first path ($l = 1$ and $\ell = 1$) as the strongest LOS path, and the remaining paths are scattered according to an uniform distribution, such that $\tau_a^l \sim \mathcal{U}\left[\tau_a^1, 2\tau_a^1\right]$, as illustrated in Table I; the exception being the direct channel delays, τ_d^l, which are all scattered after the same fashion. Furthermore, Table I shows also that the azimuth (ϕ_a and ϕ_b) and elevation (φ_a and φ_b) angles can vary randomly around the LOS path initial angle, according to $\mathcal{U}\left[-40°, 40°\right]$ and $\mathcal{U}\left[-10°, 10°\right]$ distributions, respectively. Finally, observe in Table I that the propagation losses α^l and β^ℓ take into account the following: (i) the effective aperture achieved between the RIS elements and the isotropic antennas of both the AP and UE; (ii) the large-scale and small-scale path losses and (iii) the so-called Rice factors for the LOS path.

B. Performance Analysis

Before presenting the results, we introduce the so-called coherent rate, which serves as an upper bound to the achievable rate, and is described by the following expression

$$R_{\mathrm{C}} = \frac{B}{\xi}\sum_{i=0}^{K-1} \log_2\left(1 + \frac{p_i}{BN_0}\left(\left|\mathbf{f}_i^{\mathrm{H}}\mathbf{h}_d\right| + \left\|\mathbf{f}_i^{\mathrm{H}}\mathbf{V}^{\mathrm{T}}\right\|_1\right)^2\right) \ \text{bit/s}, \tag{15}$$

TABLE I

FIXED PARAMETERS OF THE CHANNEL MODEL. OBSERVE THAT $u \sim \mathcal{U}[0,1]$ AND $n \sim \mathcal{N}(0,1)$.

General Parameters		Channel Parameters		Channel Parameters	
Parameter	**Value**	**Parameter**	**Value**	**Parameter**	**Value**
$(x_a,\, y_a,\, z_a)$	$(40,\, -200,\, 0)$ meters				
$(x_b,\, y_b,\, z_b)$	$(20,\, 0,\, 0)$ meters				
M	$\lfloor B\left(2\tau_a^1 + 2\tau_b^1 - \tau_d^1\right)\rceil + 11$ samples	α^l and β^ℓ	$\alpha^l = \gamma^l \frac{d_H d_V}{\lambda^2/4\pi} 10^{\frac{-30.18-26\log(d_a)}{10}}$; $\gamma^1 = \frac{\omega_R}{1+\omega_R}$, $\omega_R = 10^{\frac{13-0.03 d_a}{10}}$; $\gamma^l = \frac{\omega_P^l}{\sum_{\forall l} \omega_P^l (1+\omega_R)}$, $\omega_P^l = 10^{-\tau_a^l + 0.2n}$, $\forall l > 1$	τ_a^l and τ_b^ℓ	$\tau_a^1 = \frac{\overbrace{\lVert (x_a,\, y_a,\, z_a) \rVert_2^2}^{d_a}}{3\times 10^8}$; $\tau_a^l = \tau_a^1 (1+u)$, $l \in \{2,\ldots,L_a\}$
f_c	3 GHz				
$d_{\mathrm{H}} = d_{\mathrm{V}}$	0.25λ meters				
N_0	$10^{\frac{-164\ \mathrm{dB}}{10}} \times 10^{-3}$ W/Hz				
L_a	101 paths	$\boldsymbol{\phi}_a$ and $\boldsymbol{\phi}_b$	$\phi_a^1 = \arctan(y_a/x_a)$; $\phi_a^l = \phi_a^1 + \frac{40\pi}{180}(2u-1)$, $\forall l > 1$	$\boldsymbol{\varphi}_a$ and $\boldsymbol{\varphi}_b$	$\varphi_a^1 = 0$; $\varphi_a^l = \frac{10\pi}{180}(2u-1)$, $\forall l > 1$
L_b	51 paths				
L_d	100 paths				

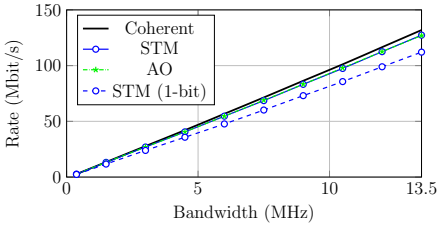

Fig. 2. Estimation of the achievable rate for multiple bandwidth values.

in which one can notice that the direct channel coefficients sum coherently with the composite channel counterparts; thus the rate achieved in (15) represents the maximum channel capacity achievable for the respective scenario discussed.

Furthermore, recall that in this work we also discuss performance results when there is a discrete number of configurations for the phase-shifts. This means that phase quantization can be applied directly to the AO or STM methods. Considering the aforementioned, we then have the quantization operation being represented by

$$\boldsymbol{\theta}^q = \lfloor \boldsymbol{\theta}/\Delta \rceil \times \Delta \ ; \ \Delta = \pi/2^{(b-1)}, \tag{16}$$

where $\boldsymbol{\omega}_{\theta^q} = e^{\jmath \boldsymbol{\theta}^q}$ describes the discretized RIS configuration and the number of bits or levels of quantization is given by b-bit(s).

1) Achievable Rate and Bandwidth: Figure 2 shows the rate achieved for a range of bandwidth (B) values or, alternatively, for an increasing number of OFDM subcarriers employed in signal transmission, and the RIS is configured by the methods discussed in Subsection II-B. Moreover, note that for Figure 2, the number of RIS reflectors was chosen to be $N = 400$, in which $N_{\mathrm{row}} = N_{\mathrm{col}} = 20$ and that each simulation point was generated with 200 Monte Carlo realizations of the channel model.

Therefore, observe in Figure 2 that the STM method is remarkably efficient since it presents an equal rate to that of the AO framework for all the bandwidth range analyzed. Beyond that, notice how both of the RIS configurations shown in Figure 2 are capable of achieving rates relatively close to the upper bound given by the coherent rate. However, this relative performance of both the STM and AO drops as the bandwidth increases. This can be explained by the fact that larger bandwidth means more OFDM subcarriers, which in turn implies that it is more difficult for a given RIS configuration to reach a satisfactory trade-off between all subcarriers. Finally, note also in Figure 2 that the 1-bit quantized [11] STM presents a sensible loss of perfomance, as expected.

In the next subsection, we present more results regarding the discretized RIS configurations, alongside with the introduction of alternative performance metrics.

2) Relative Rate, Efficiency Rate, and Number of Reflectors: To obtain comprehensive results for the performance analysis through the achievable rate, we propose the relative rate and define it according to the following

$$R_{\mathrm{Rel.}} = {}^{R_{\mathrm{A}}}/_{R_{\mathrm{C}}} \times 100\%, \tag{17}$$

wherein R_{A} is the achievable rate of a given method as, for example, the STM or AO, and R_{C} is given by (15). Note that, as mentioned before, the maximum achievable rate is given by R_{C}. More importantly, this metric provides a simpler template for performance analysis, particularly when small differences in performance are concerned, as will become clear later.

Although the achievable rate is an important metric for performance analysis, the overhead or complexity for configuring the RIS should also be discussed. In this work, we propose to relate this complexity, to the frequency with which each RIS element need to change its phase configuration between channel realizations. In other words, if $I^{r,r'}$ computes the number of RIS reflectors or elements that changed their phase configuration between adjacent channel realizations r and r', then we have the so-called efficiency rate given by

$$R_{\mathrm{Eff.}} = \left(1 - \left\langle I^{r,r'} \right\rangle\right) \times 100\%, \tag{18}$$

where R is the total number of channel realizations. Thus, $R_{\mathrm{Eff.}}$ increases as fewer RIS elements need to modify their phase-shifts for each new channel realization, meaning that in general fewer resources are spent configuring the RIS [12].

In Figures 3 (a) and (b) the values of $R_{\mathrm{Rel.}}$ and $R_{\mathrm{Eff.}}$ are, respectively, plotted against a range of reflector numbers for the RIS. More specifically, in Figure 3 (a) the relative performance given by $R_{\mathrm{Rel.}}$ is generated for $B = 10.5$ MHz and also $B = 4.5$ MHz where indicated, with the levels of quantization (see (16)) 1-bit, 2-bit, 4-bit and 16-bit. Important to mention, however, that the AO method attained a similar

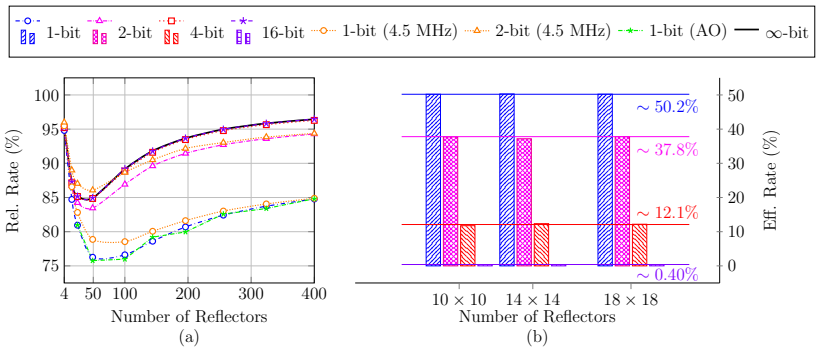

Fig. 3. (a) estimation of $R_{\text{Rel.}}$ for a range of numbers of reflectors; (b) and of $R_{\text{Eff.}}$ for three different RIS sizes ($N_{\text{row}} \times N_{\text{col}}$) with $R = 5 \times 10^3$.

performance to that of the STM for all the aforementioned quantization levels. Therefore, such redundant performance results aside from the 1-bit quantization were omitted for the sake of brevity. Moreover, the ∞-bit notation is used to indicate that phase configuration is continuous.

Therefore, note in Figure 3 (a) that, for all methods and quantization levels, the relative performance initially decreases as the number of reflectors increases, but it then increases asymptotically for larger values of the reflector number. This asymptotic improvement of the relative performance occurs approximately for $R_{\text{Rel.}} > 50$ reflectors and it is expected, given that with more reflectors, more reflection paths are established and also an increased diversity for the RIS configuration is available [2]. However, the better initial relative performance (for $R_{\text{Rel.}} < 25$) can be explained by the absolute achievable rate being exceedingly low even for the upper bound ($R_{\text{C}} \approx 40$ Mbit/s for $B = 10.5$ Mhz). This has the effect of restricting the range of achievable rates and bringing the relative performances close to each other. Therefore, this range of number of reflectors is prohibitive in practice and a greater number of them is necessary to justify the use of RIS.

Furthermore, Figure 3 (a) shows that not only the quantization causes a general loss of performance (see Figure 2), but it also enhances the aforementioned initial decrease in the performance. This happens because the errors introduced by the quantization are more prevalent for a lower number of reflectors and, as this number increases, the impact the quantization errors are diminished. Although the quantization errors are always present, if a sufficient number of levels are used, then the relative performance with quantization can be approximately identical to the case where the phase shift is continuous (see 16-bit in Figure 3 (a)). Finally, observe also in Figure 3 (a) that the relative performance is indeed better for lower bandwidths, where the same conclusion can be drawn from Figure 2.

IV. Conclusions

In this work, we introduced the RIS as a mechanism for controlling the signal propagation in a wideband communications system. To analyze the effectiveness of the RIS, we first presented a detailed channel model followed by different methods for configuring the RIS phase-shifts. Our findings indicate that the STM method delivers the best performance-complexity trade-off across different bandwidths, since the AO method relies on complicated SCA approximations. We also discussed results considering discrete or quantized phase-shifts. These results showed that if enough quantization bits are used, then the associated quantization loss becomes negligible. Moreover, it was demonstrated that quantization can lower the RIS configuration overhead, which adds flexibility to the RIS specification and allows for a more precise trade-off between the RIS performance and configuration overhead. In conclusion, for future works it would be interesting to analyze NLOS scenarios for the channel model and also explore other methods for configuring the RIS.

References

[1] I. F. Akyildiz, A. Kak, and S. Nie, "6G and Beyond: The future of wireless communications systems," *IEEE Access*, vol. 8, pp. 133 995–134 030, 2020.

[2] E. Björnson, H. Wymeersch, B. Matthiesen, P. Popovski, L. Sanguinetti, and E. de Carvalho, "Reconfigurable Intelligent Surfaces: A signal processing perspective with wireless applications," *IEEE Signal Process. Mag.*, vol. 39, no. 2, pp. 135–158, 2022.

[3] B. Feng, J. Gao, Y. Wu, W. Zhang, X.-G. Xia, and C. Xiao, "Optimization techniques in reconfigurable intelligent surface aided networks," *IEEE Wirel. Commun.*, vol. 28, no. 6, pp. 87–93, 2021.

[4] C. Pan, G. Zhou, K. Zhi, S. Hong, T. Wu, Y. Pan, H. Ren, M. D. Renzo, A. Lee Swindlehurst, R. Zhang, and A. Y. Zhang, "An overview of signal processing techniques for RIS/IRS-aided wireless systems," *IEEE J. Sel. Top. Signal Process.*, vol. 16, no. 5, pp. 883–917, 2022.

[5] C. You, B. Zheng, and R. Zhang, "Channel estimation and passive beamforming for intelligent reflecting surface: Discrete phase shift and progressive refinement," *IEEE J. Sel. Areas Commun.*, vol. 38, no. 11, pp. 2604–2620, 2020.

[6] R. Dong, Y. Teng, Z. Sun, J. Zou, M. Huang, J. Li, F. Shu, and J. Wang, "Performance analysis of wireless network aided by discrete-phase-shifter IRS," *J. Commun. Netw.*, vol. 24, no. 5, pp. 603–612, 2022.

[7] D. Gunasinghe and G. Amarasuriya, "Best IRS selection versus distributed IRS with phase-shift errors," in *2022 IEEE Glob. Commun. Conf. (GLOBECOM)*, 2022, pp. 4032–4037.

[8] Y. Yang, B. Zheng, S. Zhang, and R. Zhang, "Intelligent reflecting surface meets OFDM: Protocol design and rate maximization," *IEEE Trans. Commun.*, vol. 68, no. 7, pp. 4522–4535, 2020.

[9] E. Bjornson, P. Zetterberg, M. Bengtsson, and B. Ottersten, "Capacity limits and multiplexing gains of MIMO channels with transceiver impairments," *IEEE Commun. Lett.*, vol. 17, no. 1, pp. 91–94, 2013.

[10] S. Diamond and S. Boyd, "CVXPY: A Python-embedded modeling language for convex optimization," *J. Mach. Learn. Res.*, vol. 17, no. 83, pp. 1–5, 2016.

[11] A. Mudonhi, M. Lotti, A. Clemente, R. D'Errico, and C. Oestges, "Ris-enabled mmWave channel sounding based on electronically reconfigurable transmitarrays," in *2021 15th European Conf. on Antennas and Propag. (EuCAP)*, 2021, pp. 1–5.

[12] C. Liaskos, L. Mamatas, A. Pourdamghani, A. Tsioliaridou, S. Ioannidis, A. Pitsillides, S. Schmid, and I. F. Akyildiz, "Software-Defined Reconfigurable Intelligent Surfaces: From theory to end-to-end implementation," *Proc. IEEE*, vol. 110, no. 9, pp. 1466–1493, 2022.